Development of a hysteresis model based on axisymmetric and homotopic properties to predict moisture transfer in building materials

Ahmad Deeb, Ferhat Benmahiddine, Julien Berger, Rafik Belarbi

Development of a hysteresis model based on axisymmetric and homotopic properties to predict moisture transfer in building materials

Ahmad Deeb[a,*], Ferhat Benmahiddine[b,c], Julien Berger[b], Rafik Belarbi[b,c,d]

November 9, 2023

[a] Department of Mathematics, Khalifa University, Abu Dhabi, United Arabes of Emirates.
[b] Laboratoire des Sciences de l'Ingénieur pour l'Environnement (LaSIE), UMR 7356 CNRS, La Rochelle Université, CNRS, 17000, La Rochelle, France.
[c] 4ev Lab, Laboratoire des Sciences de l'Ingénieur pour l'Environnement (LaSIE), CNRS, EDF R&D, CNR, La Rochelle Université, Avenue Michel Crépeau 17042 La Rochelle Cedex1, France.
[d] Department of Civil Engineering, Université de Sherbrooke, 2500 Bd. de l'Université, Sherbrooke QCJ1K2R1, Canada.
[*] ahmad.deeb@ku.ac.ae

Abstract

Current hygrothermal behaviour prediction models neglect the hysteresis phenomenon. This leads to a discrepancy between numerical and experimental results, and a miscalculation of buildings' durability. In this paper, a new mathematical model of hysteresis is proposed and implemented in a hygrothermal model to reduce this discrepancy. The model is based on a symmetry property between sorption curves and uses also a homotopic transformation relative to a parameter $s \in [0, 1]$. The advantage of this model lies in its ease of use and implementation since it could be applied with the knowledge of only one main sorption curve by considering $s = 0$, in other words, we only use the axisymmetric property here. In the case where the other main sorption curve is known, we use this curve to incorporate the homotopy property in order to calibrate the parameter s. The full version of the proposed model is called *Axisymmetric+Homotopic*. Furthermore, it was compared not only with the experimental sorption curves of different types of materials but also with a model that is well known in the literature (Carmeliet's model). This comparison shows that the Axisymmetric+Homotopic model reliably predicts hysteresis loops of various types of materials even with the knowledge of only one of the main sorption curves. However, the full version of Axisymmetric+Homotopic model is more reliable and covers a large range of materials. The proposed model was incorporated into the mass transfer model. The simulation results strongly match the experimental ones.

Key words: Hysteresis modelling; Homotopy; axisymmetry; moisture sorption; porous material; heat and mass transfer.

1 Introduction

Heat and moisture transfer has a significant impact on a building's energy performance and durability [1, 2]. Moisture affects the comfort of the occupants and the indoor air quality of the living environment. Moreover, water is a transporter of aggressive agents [3] such as chlorides and sulphates. Its presence inside a material is a facilitator for fungal growth. Also, it is the main product of chemical reactions such as carbonation. This makes the process of mass transfer (especially of humidity) increasingly important as it can change the overall balance of a building. The modelling of these phenomena remains complex [4] to the point where significant inconsistencies are observed between simulation results and experimental data. These inconsistencies are attributed to certain assumptions in the hygrothermal behaviour model, mainly the non-inclusion of the hysteresis phenomenon between adsorption and desorption curves [5–8].

Experimental studies show that water sorption isotherms, which require a long period of time to be registered [9, 10], are not the same in adsorption and desorption, which gives rise to hysteresis behaviour in both processes. This can have several explanations such as the variation of the liquid-solid contact angle, the radius of curvature of the fluid-vapour interface, and the ink bottle effect [11–13]. Thus, in the computational modelling, the water content to be considered, at a given level of relative humidity, is between

the adsorption and desorption values associated with this humidity level due to the hysteresis effect. This means that simulating the hygrothermal behaviour of such a material under dynamical climate conditions considering only the main adsorption or desorption curve would lead to significant deviations between the numerical and experimental results [14]. Indeed, the main sorption curves do not describe the real hydric behaviour of a material. The former are simply the maximum and minimum amounts of water that a material can bear [13, 15–18]. The actual water content of the material will depend on its thermo-hydric history, in addition to the real climate conditions [13, 19, 20], and it will be represented by intermediary curves located between the main sorption ones.

Many studies have been conducted in order to take into account the hysteresis phenomenon in the modelling of the hygrothermal behaviour of materials, of which we mention some. [21] reformulated the Parlange hysteresis model as a pair of recurrence formulas to provide relations between wetting and drying phases up to any order. [17] proposed a model based on the Van-Genuchten one and the main experimental sorption curves to generate a series of wetting and drying scanning curves. [22] modified the Parker-Lenhard (PL) method in the Kool-Parker (KP) soil moisture hysteresis model to eliminate any artificial pumping errors. [23] proposed a hysteresis model for moisture content in wood, which mathematically resolves as closed-form expressions. Other studies were also presented in [18, 24–29]

To summarise, [14] showed that taking into account the intermediary sorption curves of hemp concrete gives better results than if only the main sorption loop was considered. [8] have recently shown that hysteresis has a significant effect on the numerical prediction in the short-term, and that taking this phenomenon into account leads to an improvement in the quality of the prediction of numerical models. In addition, [5] proved that including only one of the sorption isotherm equations in the modeling leads to significant differences between the numerical and experimental results. Furthermore, they also showed in [5] that neglecting the hysteresis phenomenon in the case of realistic climate conditions leads to an overestimation of the moisture buffering properties of materials in contact with indoor air. This may lead to an underestimation of the risks of mould growth and condensation of water, thus causing durability problems [6]. This has also been confirmed by [30].

There are three types of hysteresis models in the literature, [31, 32]. The first are physical ones such as Carmeliet's model [33], which is based on Mualem's model [15]. The second are mathematical models such as Huang's model [17], which is based on Kool and Parker's model [34], which, in turn, is based on Scott's model [35]. Finally, we have the empirical models like Pedersen's model [36].

Huang's model [17] was developed under the assumption that the residual water content (corresponding to a relative humidity $\phi = 0$) is the same in adsorption and desorption. This remains valid in the case of water saturation (relative humidity $\phi = 100\%$) [37]. As for the model of Kool and Parker [34], they assume that the shapes of the main and intermediary curves are similar. From another point of view, Mualem's physical model II is based on two main assumptions: similarity and independent domain [33, 38]. In this model, It is assumed that there is no interaction between the pores of a porous material [37]. This physical model explains the shape of the intermediary curves by physical properties such as pore radius distribution, [15, 31]. In general, physical and mathematical models are predictive. Their model only requires knowledge of the main adsorption and desorption curves. This is the same for Pedersen's empirical model.

The prediction of the hygrothermal behaviour of materials is linked to the type of hysteresis model chosen. [31] compared the pertinence of various hysteresis models. He demonstrated that, contrary to physical and mathematical models, whatever the adjustment parameters chosen for the empirical models, they do not respect the condition of closing the adsorption/desorption curves. He added that Pedersen's model leads to an overestimation of the water content during looping. In addition, a comparative study that was conducted by [12] concluded that empirical models provide better predictions of water content, but pumping errors (PEs) cannot be avoided. In another study, [19] carried out a comparative study between a physical (Mualem II) and an empirical (Robien) model. They concluded that the performance of the physical model was better due to the pumping effects present in the empirical model. They recommended Mualem Model II for hygrothermal transfer modelling in cementitious materials exposed to dynamic climate conditions. Recently, [13] proposed a model that introduces the concept of the gripped-box. The advantage of this model is that it requires only two parameters to be adjusted and allows the closure of the sweeping

loops (avoids the pumping effect) in each humidification/drying cycle.

This work proposes a reliable model for the influence of the hysteresis phenomenon on the mechanisms of moisture transfer in porous materials. This model is based on the idea that the main sorption and intermediary curves are considered to be symmetric relative to a given point. Taking into account this hypothesis implies that if one of the main experimental curves is known, the other could be obtained with an axisymmetric operation on the former. If this is sufficient, the time required to explore sorption curves experimentally is reduced by half. This is not the case with models in the literature such as Carmeliet's model, [39], which requires that both main sorption curves to be calculated. However, when the two main sorption curves are known, the proposed model is updated by adding a homotopic operation to improve the prediction. This homotopic function, which depends on a parameter s, proposes that if one main sorption curve is known, the other is not its axisymmetric, as supposed above, but lies between the main sorption curve and its axisymmetric. This updated version is called in the following *Axisymmetric+Homotopic (s)* model. If only one main sorption curves is known, then the model uses only the axisymmetric property, thus $s = 0$ and there is no effect of the homotopic transformation. If both main sorption curves are known, then the model uses in addition the homotopic transformation and thus $s \neq 0$.

This is not the only contribution. As our main goal was to predict the behaviour of cementitious materials, and to improve the modelling and simulation for the hygrothermal problems of porous materials that are exposed to dynamic boundary conditions, the proposed model was generalized and adapted in order to obtain the intermediary sorption curves associated to the materials, so it can enable producing intermediary curves while ensuring the property of continuity. In other words, when the material changes its state from wetting/drying to drying/wetting, the moisture content must be the same. This is not verified by some empirical models in the literature, such as the Zhang model, [12]. The Axisymmetric+Homotopic model verifies the continuity property and ensures that moisture content is the same at any inversion point.

This article is structured as follows: for the sake of clarity, we start at the beginning of the next section by presenting the axisymmetric proposition between sorption curves. Then, the homotopic function part of the model is introduced at the end of the following section. Two cases of the proposed model are applied: the case when there is no use of the homotopic transformation ($s = 0$) and the case when s is calibrated with the use of the second experimental main sorption curve. First, we ran them both to produce the intermediary curves of the Polystyrene materials. Then, we made a series of experiments with different materials (Argil, raw earth, brick, OSB1 and hard stone) that test how efficient they are in producing main and intermediary sorption curves. The results were compared with the experimental data and numerical predictions that were produced by Carmeliet's model. The modelling of mass transfer was then elaborated for cementitious materials, and the numerical tools that were used to solve the mathematical model are briefly described. We end by incorporating the Axisymmetric+Homotopic model into the simulation in order to see how efficiently this takes into account the hysteresis effect. Numerical outputs of the simulation of the model of mass transfer, with and without taking into account the hysteresis phenomenon in different models, were compared with experimental results. This was done for two materials, hemp concrete and Tradical, that were subjected to different hydric dynamics conditions.

2 Methodology

Experimental investigations of gas adsorption in materials [40] have shown that sorption curves can be classified into 4 types, where one extreme has mostly a vertical shape and another extreme has mostly a horizontal one. The other types may be regarded as intermediary curves between the two extremes. This observation led us to propose that, if one of the main sorption curve has been determined, the other is either its symmetric of the first with respect to a specific point, which led us to define a model based on a symmetry property, or it is bounded between the already obtained curve and its symmetry. However if both main sorption curves are known, the model uses the homotopy property. The property of symmetry with respect to a specific point will be called "axisymmetric" throughout this work.

In this section, a proposition to model the hysteresis phenomenon and its dynamics within hydric variations is demonstrated. This relies on the assumption that the hysteresis phenomenon has an axisymmetric

property between the adsorption and desorption curves, which would help predict hysteresis loops where only one main sorption curve is given. This it could cover specific types of materials, as is shown later.

2.1 Hysteresis in porous materials

The sorption curves of a material link the moisture content w to the relative humidity ϕ. An illustration of hysteresis for the moisture content in porous materials is presented in Figure 1(d). If a completely dry material is submitted to an increase in relative humidity, the change in moisture content will follow the main adsorption one, as shown in Figure 1(a). Then, if the material is dried by imposing a lower relative humidity, the moisture content in the material is given by an intermediary desorption curve, different from the main desorption curve (Figure 7). Thus, the moisture content in the material is subjected to hysteresis effects. In other words, the moisture content depends on the change over time of the relative humidity.

For $w\ [-]$ being the normalized moisture content and $\phi\ [-]$ the relative humidity, both defined on $[\,0\,,\,1\,]$, where the value 0 describes the absence of water and 1 its full presence, the adsorption and desorption curves are defined by the following functions:

$$w_{a,i} : \phi \longmapsto w_{a,i}(\phi)\,, \qquad \frac{\partial \phi}{\partial t} > 0\,, \tag{1}$$

$$w_{d,i} : \phi \longmapsto w_{d,i}(\phi)\,, \qquad \frac{\partial \phi}{\partial t} < 0\,, \quad i \in \mathbb{N}\,. \tag{2}$$

Here, for every element ϕ that belongs to $[0,1]$, the operator $\longmapsto$ produces an image that also belongs to $[0,1]$. Here, i represents the number of hysteresis loops. By convention, $i = 0$ stands for the main adsorption and desorption curves and $i > 0$ for the intermediary ones.

2.2 Hysteresis model based on the axisymmetric property

The main idea of our model is based on the axisymmetric property between the adsorption and desorption curves. To illustrate this point simply, the following transformation is considered:

$$\mathcal{T} : w(\phi) \longmapsto 1 - w\,(1 - \phi)\,. \tag{3}$$

This transformation enables us to obtain the desorption curve starting from the adsorption one as illustrated in Figure 1.

Considering the adsorption curve $w(\phi)$ $(\forall\, \phi \in [0,1])$ in Figure 1(a), if one operates the transformation $w\,(1 - \phi)$, this gives the curve shown in Figure 1(b). Then, by carrying out successively $-\,w\,(1 - \phi)$ and $1 - w\,(1 - \phi)$, this leads to the desorption curve illustrated by the dashed red line in Figure 1(d). It can be proven that:

$$\mathcal{T}\Big(\mathcal{T}\big(w(\phi)\big)\Big) = w(\phi)\,. \tag{4}$$

Thus, the transformation is reversed. In other words, the desorption curve can be constructed from the adsorption curve and vice versa. Relying on this property, the model ensures the presence of the closure points phenomenon for experimental sorption curves. This means that, starting from a fully dry state, if we fully wet the material to reach full saturation and then we completely dry it, we would reach the initial completely dry state.

Now, the generalization of such a transformation will be presented to produce intermediary curves. Let us assume that the material was in an intermediary wetting process at $\phi_i \in [\,0\,,\,1\,]$ and it is going to be dried out $(\dfrac{\partial \phi}{\partial t} < 0)$; in other words we have an intermediary adsorption curve $w_{a,i}$ and we need to determine the associated intermediary desorption curve $w_{d,i}$. The latter is given by:

$$w_{d,i}(\phi) = \mathcal{T}_d\left(w_{a,i}(\phi)\right), \tag{5}$$

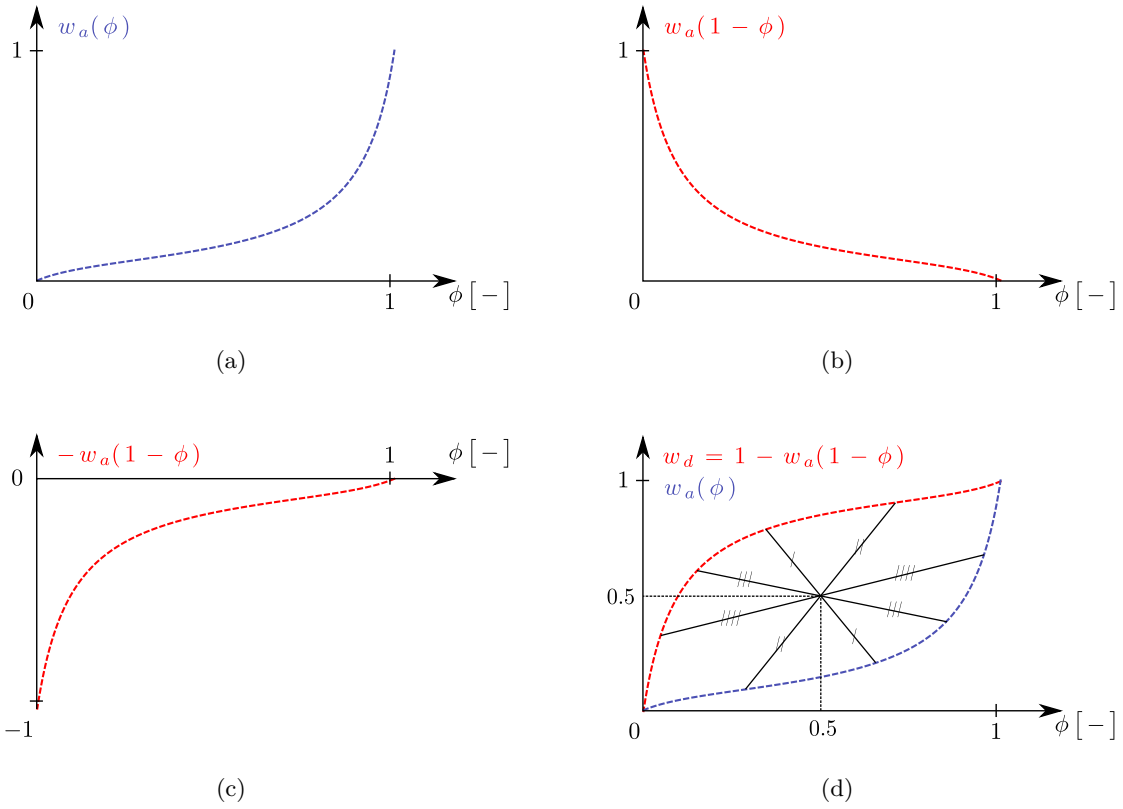

Figure 1. *Basic idea of the axisymmetric transformation to obtain the desorption curve* (d) *starting from the adsorption curve* (a) *through intermediary transformations (*(b) *and* (c)*).*

with the following transformation:

$$\begin{aligned} \mathcal{T}_d \,:\, [\,0\,,\,\phi_i\,] &\longrightarrow [\,0\,,\,1\,] \\ \phi &\longmapsto \mathcal{T}(\,w_{a\,,i}\,(\phi)\,)\cdot s_d\,, \end{aligned} \tag{6}$$

where the scaling parameter s_d is introduced to ensure the continuity of the transition between the two curves $w_{a\,,i}\,(\,\phi\,)$ and $\mathcal{T}_d(\,w_{a\,,i}\,(\phi)\,)$. This is given by:

$$s_d \overset{\text{def}}{:=} \frac{w_{a\,,i}\,(\,\phi_i\,)}{\mathcal{T}(\,w_{a\,,i}\,(\phi_i)\,)}\,. \tag{7}$$

Here, the index i stands for the number of the hysteresis loops in the experiment. Conversely, if we now wish to wet $(\frac{\partial\,\phi}{\partial t} \,>\, 0\,)$ the material after a drying process at $\phi_i \,\in\, [\,0\,,\,1\,]$, the intermediary adsorption curve is given by:

$$w_{a\,,i+1}\,(\phi) \;=\; \mathcal{T}_a\,(\,w_{d\,,i}\,(\phi)\,)\,, \tag{8}$$

with the following transformation of the desorption curve:

$$\begin{aligned} \mathcal{T}_a \,:\, [\,\phi_0\,,\,1\,] &\longrightarrow [\,0\,,\,1\,] \\ \phi &\longmapsto s_a\cdot\mathcal{T}(\,w_{d\,,i}\,(\phi)\,) \,+\, 1 \,-\, s_a\,, \end{aligned} \tag{9}$$

where the scaling parameter s_a ensures the continuity condition, and it is defined as: $\mathcal{T}_a(\,w_{d\,,i}(\,\phi_i\,)\,) \;=\; w_{d\,,i}(\,\phi_i\,)$.

$$s_a \overset{\text{def}}{:=} \frac{w_{d\,,i}(\,\phi_0\,) \,-\, 1}{\mathcal{T}(\,w_{d\,,i}(\,\phi_0\,)\,) \,-\, 1}\,. \tag{10}$$

It should be noted that the starting main sorption curve can be determined by fitting analytical expressions into experimental measurements using least square methods [41]. In this paper, the main adsorption curve was used as a starter in the proposed model.

2.3 Dynamical conditions

Here, a simple example is presented to understand how the hysteresis paths are defined for dynamic boundary conditions. The issue is to determine the adsorption $w_{a\,,i}(\,\phi\,)$ and desorption $w_{d\,,i}(\,\phi\,)$ curves for 9 cycles of drying and wetting induced by the dynamics of relative humidity, as given in Figure 2. At the initial state, the material is completely dry $\phi_0 \;=\; 0$. The first cycle is wetting $\frac{\partial\phi}{\partial t} \,>\, 0$. To predict the water content value associated with this process, the following Van–Genuchten model was employed:

$$w_{a\,,0} \;=\; \frac{\pi}{\left(\,1 \,+\, (\,-\,\alpha^{-1}\cdot c\,)^{\frac{1}{1\,-\,m}}\right)^{m}}\,, \tag{11}$$

where $c \overset{\text{def}}{:=} -\frac{\rho_2\,R\,T}{M_2}\;\ln\phi\;[\,\mathsf{Pa}\,]$ is the suction pressure, π is the porosity of the material, and the two constants m and α are the parameters that we adjust in order to fit the experimental values of the sorption curves. Then, at $\phi_1 \;=\; 1$, the fully saturated material undergoes a drying process $\frac{\partial\phi}{\partial t} \,<\, 0$. In order to determine the main desorption curve, we used the following transformation:

$$\begin{aligned} w_{d\,,0}\,(\phi) \;&=\; \mathcal{T}_d(\,w_{a\,,0}\,(\phi)\,) \\ &=\; s_d\cdot\Big(\,1 \,-\, w_{a\,,0}(\,1 \,-\, \phi\,)\Big)\,. \end{aligned} \tag{12}$$

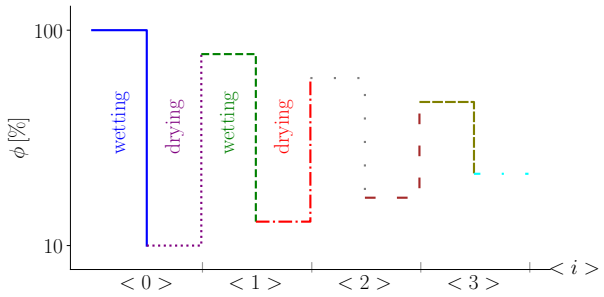

Figure 2. *Dynamic variation of the relative humidity of a material during the drying and wetting processes.*

For $m = 0.414$ and $\alpha = 0.9 \times 10^7$, the resulting curve is illustrated by the black dotted line in Figure 3(a). The material was then dried until $\phi_2 = 0.1$, before undergoing another wetting process. Then, the intermediary adsorption curve is given by:

$$\begin{aligned} w_{a,1}(\phi) &= \mathcal{T}_a(w_{d,0}(\phi)) \\ &= s_a \cdot \Big(1 - w_{d,0}(1-\phi)\Big) + 1 - s_a, \end{aligned} \tag{13}$$

which is illustrated by the green dashed line in Figure 3(c). The wetting process was stopped at $\phi_2 = 0.9$, and then the intermediary desorption curve is given by:

$$\begin{aligned} w_{d,1}(\phi) &= \mathcal{T}_d(w_{a,1}(\phi)) \\ &= s_d \cdot \Big(1 - w_{a,1}(1-\phi)\Big). \end{aligned} \tag{14}$$

This curve is illustrated by the red dashed dotted line in Figure 3(c). The curve can then be determined during the successive drying and wetting processes as shown in Figure 3(e) and 3(g). Note that the methodology is independent from the fitting model chosen for the initial adsorption curve. In other words, we have the freedom to choose any function we want as long as it satisfies the properties of the sorption curves. In Figures 3(b), 3(d), 3(f) and 3(h), the curves were determined for a third order polynomial model. As a fitting model, the main adsorption curve is:

$$w(\phi) = 2.8125\,\phi^3 - 3.5\,\phi^2 + 1.6875\,\phi. \tag{15}$$

Note that in all cases, the intermediary curves are bounded by the main sorption curves. In the next part, the homotopic transformation is incorporated in the model to present the full version of the Axisymmetric+Homotopic model.

2.4 Improved version by adding a homotopic function

Despite the fact that the above strategy can predict the intermediary curves for some types of materials (see Table 4), it fails to predict the main desorption curves via the axisymmetric property for some materials and lacks precision for others. This is because not all the main sorption curves that were taken here have an axisymmetric property, which is logical. In order to address this shortcoming, and to cover a wider range of materials for sorption curves, an homotopic function is added after the axisymmetric function.

Before going forward, let us give a short definition of a homotopic function. For two continuous functions $w_a(\phi)$ and $w_d(\phi)$ defined on the same interval $[\phi_0, \phi_1]$, such that:

$$w_a(\phi_0) = w_d(\phi_0), \qquad w_a(\phi_1) = w_d(\phi_1), \tag{16}$$

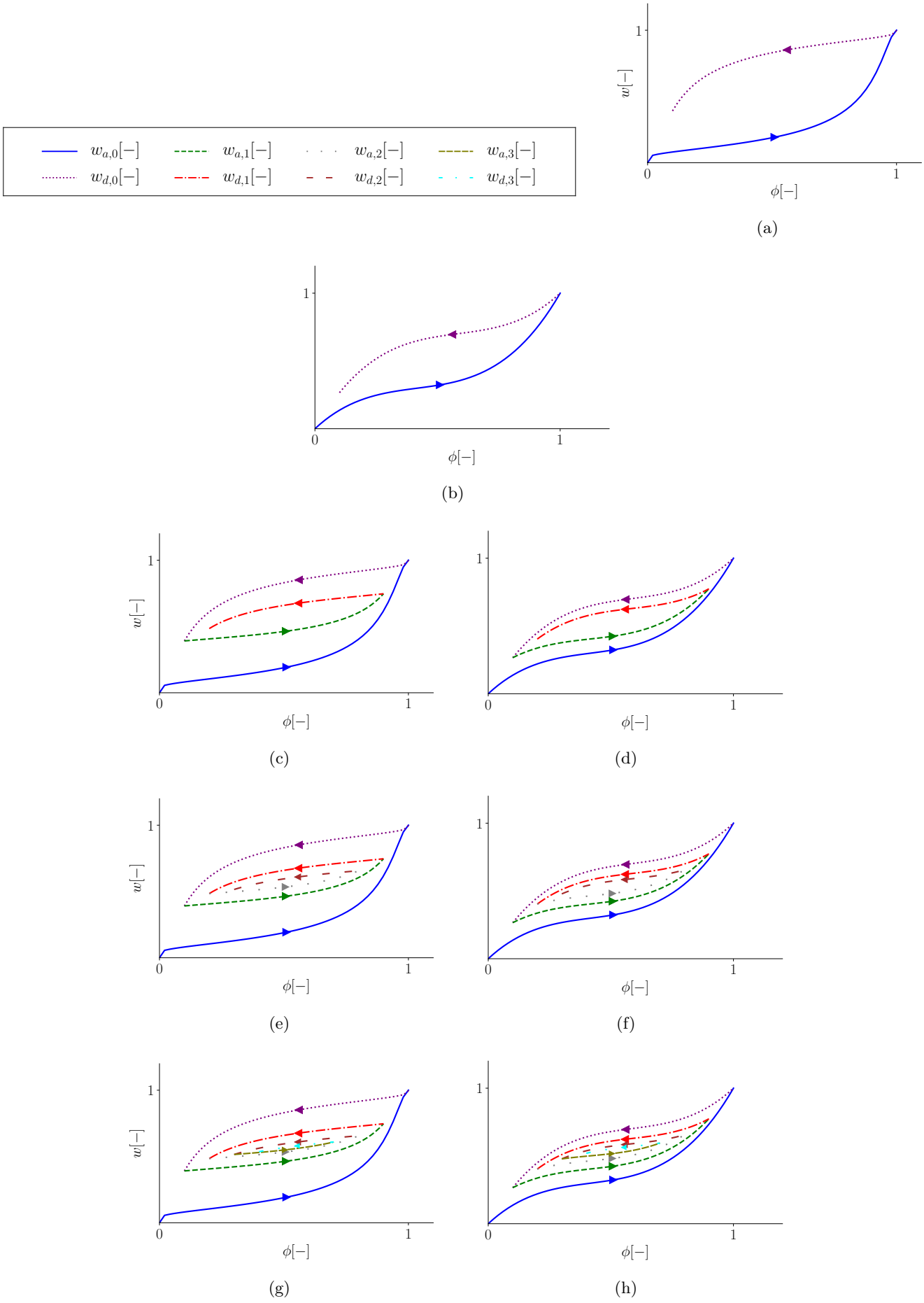

Figure 3. *Determination of the main and intermediary adsorption and desorption curves according to the dynamics of relative humidity in the* Van–Genuchten *model, as given in Figure 2, with* $m = 0.414$ *and* $\alpha = 0.9 \times 10^7$ (a,c,e,g), *and for a third order polynomial model* (15) (b,d,f,h).

we say that w, which is defined as follows for $s \in [0,1]$:

$$w : \begin{array}{ccc} [\phi_0, \phi_1] \times [0,1] & \rightarrow & [0,1] \\ (\phi\,,\, s) & \mapsto & w\,(\phi\,,\, s), \end{array} \tag{17}$$

is a homotopic function between w_a and w_d, if:

$$w\,(\phi\,, s) = (1-s)\, w_d(\phi) \;+\; s\; w_a(\phi\,). \tag{18}$$

It is simple to show that:

$$w(\,\phi\,, 0) = w_d(\,\phi), \qquad\qquad w(\,\phi\,, 1) = w_a(\,\phi), \tag{19}$$

and $w(\,\phi\,, s)$, for $s \in [0,1]$, is bounded between $w_a(\phi)$ and $w_d(\phi)$, as shown in Figure 4.

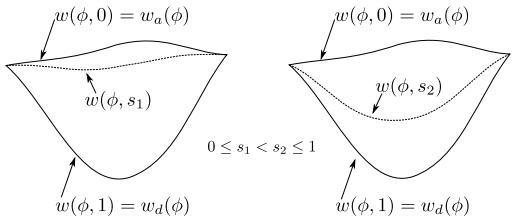

Figure 4. *Illustration of a homotopic function*

Now we will go back to the sorption curves. Knowing one of the main sorption curves, the other is considered to be the result of a homotopic function between the given main curve and its axisymmetric. In other words, if one obtains the main adsorption curve $w_{a,0}$ and its axisymmetric, as shown in Figure 1(d), the main desorption curve, depending on the parameter s, will be considered to be the function that lies between them, as shown in Figure 5. The formula for the main desorption curve is given by the following

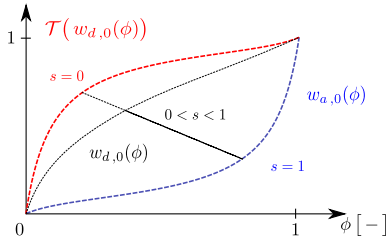

Figure 5. *Illustration of the Axisymmetric+Homotopic model that produces the main desorption curve, which is the result of a homotopic function for a fixed parameter s between the main adsorption curve and its axisymmetric*

function:

$$\begin{aligned} w_{d,0}(\phi) &= (1-s)\;\mathcal{T}(\,w_{a,0}(\phi)\,) + s\;w_{a,0}(\phi) \\ &:= \mathcal{T}_s(w_{a,0}(\phi)). \end{aligned} \tag{20}$$

This transformation is denoted by $\mathcal{T}_s$. It also ensures the presence of the closure point. Here, s is the parameter of the homotopic function which belongs to the interval $[0,1]$. For $s=0$, the result is the full axisymmetric function, as defined above in equation (5) for $i=0$ and presented in Figure 1(d), while $s=1$ produces the initial main adsorption curve $w_{a,0}(\phi)$. Adjusting s between 0 and 1 will maintain the function between $w_{a,0}$ and its transformation $\mathcal{T}(\,w_{a,0}(\phi)\,)$. This model depends then on the parameter s. To show how s affects the axisymmetric main desorption curve, Figure 6 presents the main adsorption and desorption curves for both types that were illustrated in Figure 3: Figures 6(a) and 6(c) represent the illustration of the main desorption curve obtained with a homotopic-axisymmetric transformation from the Van-Genuchten model made with $s=\frac{1}{4}$ and $s=\frac{3}{4}$, respectively, and Figures 6(b) and 6(d) are for a third order polynomial.

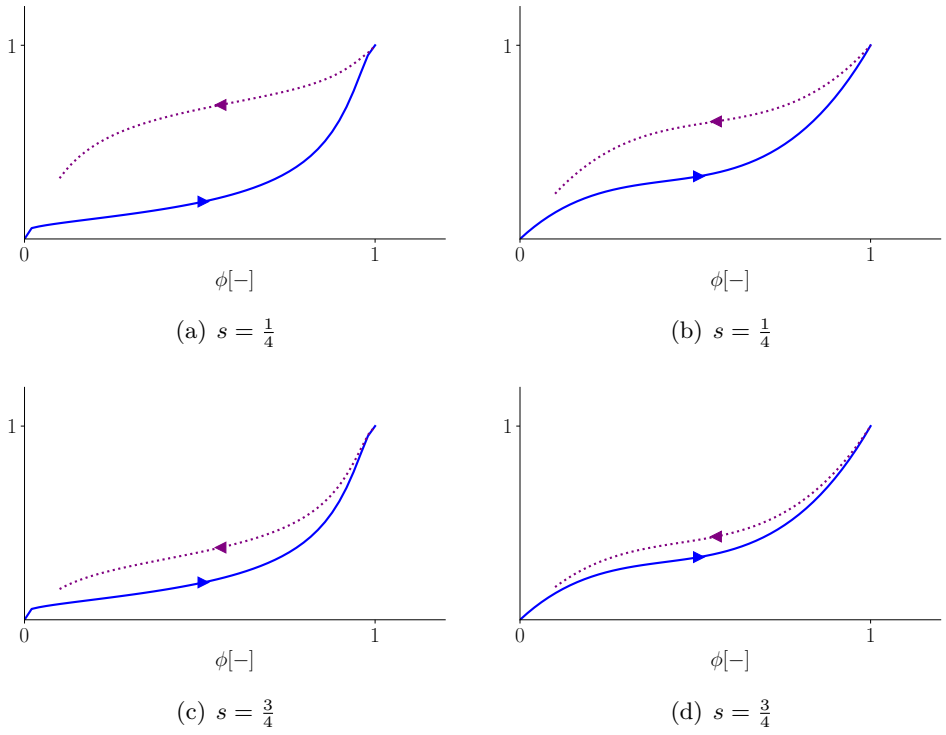

(a) $s = \frac{1}{4}$ (b) $s = \frac{1}{4}$

(c) $s = \frac{3}{4}$ (d) $s = \frac{3}{4}$

Figure 6. *Determination of the main desorption curve using a homotopic function. Illustration with two different shapes of main adsorption curves and for two different values of s.*

2.4.1 Intermediary curves.

In order to obtain the intermediary sorption curves, it is sufficient to apply the process defined in the above section, where only the axisymmetric transformation was used. Therefore, the intermediary curves are given by the following formulas:

$$\begin{aligned} w_{d,i}(\phi) &= \mathcal{T}_{d,s}\left(w_{a,i}(\phi)\right) \\ &= (1-s)\,\mathcal{T}_d\left(w_{a,i}(\phi)\right) + s\,w_{a,i}(\phi), \end{aligned} \tag{21}$$

and

$$\begin{aligned} w_{a,i+1}(\phi) &= \mathcal{T}_{a,s}\left(w_{d,i}(\phi)\right) \\ &= (1-s)\,\mathcal{T}_a\left(w_{d,i}(\phi)\right) + s\,w_{d,i}(\phi). \end{aligned} \tag{22}$$

The coefficient s is the parameter to be identified according to the experimental sorption data, where both main curves are given.

2.5 Error analysis

To analyse the quality of the numerical sorption curves, the mean absolute error of the adsorption and desorption curves at each cycle were evaluated. They are given by the following formula:

$$E_g\left(w_{a,d,i}\right) = \sqrt{\sum_{r=1}^{n^{a,d,i}} \left(w_{a,d,i}(\phi^r) - \hat{w}^r_{a,d,i} \right)^2}. \tag{23}$$

Here, the points $(\phi^r, \hat{w}^r_{a,d,i})$ for $r = 1, \ldots, n^{a,d,i}$, represent the experimental output of water content for the adsorption and desorption processes, as shown in Figure 7(b). The integer $i = 0, \ldots, 3$ is the

number referring to the cycle of the dynamic conditions that the sample is being subjected to, r is the index associated with the points that belong to the same cycle, and $n_{a,d,i}$ is the quantity of experimental data recorded during the adsorption or desorption process and for each cycle. The mean relative error was obtained by dividing the mean absolute error by the mean value of an experimental cycle, as defined in the following:

$$E_r\left(w_{a,d,i}\right) = \frac{E_g\left(w_{a,d,i}\right)}{\overline{\hat{w}}_{a,d,i}}, \tag{24}$$

$$\overline{\hat{w}}_{a,d,i} = \sqrt{\sum_{r=1}^{n_{a,d,i}} \left(\hat{w}^r_{a,d,i}\right)^2}. \tag{25}$$

3 Validation of the model with experimental sorption curves

The Axisymmetric+Homotopic model was applied and tested to predict the adsorption and desorption curves for various types of materials that underwent different wetting and drying processes. The reliability of the proposed hysteresis models was evaluated by comparison, on one hand, with experimental results, and with the Carmeliet model [33] on the other. First, we compare results that are related to the Polystyrene material. Then, a series of experiments is carried out to determine the hysteresis loops for five types of materials: Argil, Brick, Hard stone, Raw earth and OSB1 and their characteristics are presented. The Axisymmetric+Homotopic model is tested for two situations: The first with $s = 0$ and the second when s is calibrated with the two experimental main sorption curves.

3.1 Prediction of the hysteresis cycles for Polystyrene

We begin with the prediction of the wetting and drying cycles for Polystyrene. This test was carried out using the results with Polystyrene concrete characterized by Maaroufi et al. [42], where the material was subjected to different values of relative humidity from 0 % to 100 % with increment of 10 %. Between two increments, the stability of the mass of the absorbed water content was sought. Then, the material underwent a drying process from 100 % to 10 % relative humidity with the same increment; water content stability was also attained here. The latter was evaluated at the end of each increment, as shown in Figure 7(a). Then, the material was subjected to multiple cycles of wetting and drying at between 10 % and 80 % relative humidity. The water content was also measured and the values are shown in Figure 7(b). This experiment enabled us to generate experimentally the main and intermediary adsorption and desorption curves.

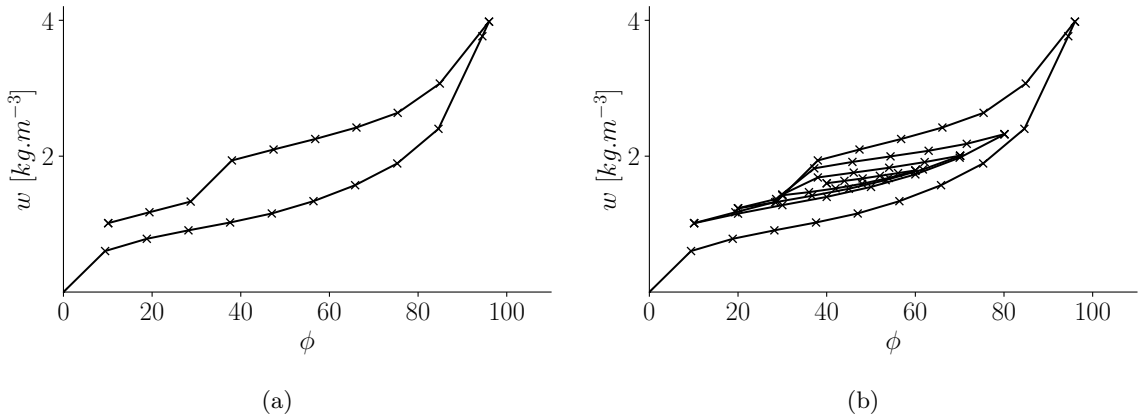

Figure 7. *Plot of the main adsorption and desorption experimental curves (a) and intermediary curves (b) of Polystyrene concrete.*

Table 1. *Parameters of the Van-Genuchten model for the main adsorption and desorption curves of Polystyrene, and the parameter s for the Axisymmetric+Homotopic.*

main adsorption		main desorption		
m	$\alpha/10^7$	m	$\alpha/10^7$	s
0.37	1.2	0.28	2.1	0.4

3.1.1 Performance with the Axisymmetric+Homotopic (s=0) model.

The Axisymmetric+Homotopic hysteresis model was used to predict hysteresis loops for $s = 0$. As it needs one of the main sorption curves, the adsorption curve was used in the model to predict the water content for the rest of the cycles. The main adsorption curve was determined by fitting experimental values with the adsorption state using the parameters of the Van-Genuchten model. The latter requires the value of the porosity, which is determined using an empirical equation, and it turns out to be equal to $\pi = 60\,\%$ [43]. The fitted parameters of model (11) for Polystyrene concrete are presented in Table 1. Note that the values of the fitted parameters relative to the experimental desorption curve are given too, as these were needed to run Carmeliet's model.

3.1.2 Performance with Axisymmetric+Homotopic ($s \neq 0$) model.

To implement the full version, the parameter s needs to be identified using the experimental main desorption curve. For the identification process, the parameter s is presented in Table 1. Therefore, the Axisymmetric+Homotopic with $s = 0.4$ model could be applied to predict hysteresis loops using formulas (21) and (22).

3.1.3 Comparison of results.

Figure 8(a) shows the hysteresis loops obtained by Axisymmetric+Homotopic (s=0) and Axisymmetric+Homotopic ($s = 0.4$) with a comparison between the experimental data and Carmeliet's model, while Figure 8(b) represents the errors of the output of these models with the experimental data. Note that in this Figure, we do not follow the same presentation as in Figures 3 and 7. However, the results are plotted according to the hysteresis cycles $< i >$ for the sake of clarity. This enables us to highlight the differences between the numerical outputs of all models on one hand and the experimental outputs on the other. We note that the use of Carmeliet's model requires knowing the two main sorption curves.

The first results show that the model having $s = 0$ and Carmeliet's model were in good agreement with the experimental observations of the main adsorption curve, as this curve was fitted for both models at the beginning. However, the discrepancies between the first desorption curve of the proposed model and the experimental values are more noticeable than those with Carmeliet's model. This is due to the fact that the main desorption curve in our model is predicted by the axisymmetric property, unlike Carmeliet's model, that requires the two main sorption curves. Otherwise, the proposed model with $s = 0$ shows less deviation than Carmeliet's model in the intermediary curves, as shown in Figure 8(b). This could be due to the fact that the fitting process for the main desorption curve came out with one that does not have the same inversion point and experimental curve. Nevertheless, when $s > 0$ is considered, results of the proposed model show a smaller error in to the main desorption curve relative to the other. This is due to the homotopic function, which gives the user the ability, by adjusting s, to be as close as possible to the main experimental desorption curve.

To analyze the performance of the proposed model, the mean absolute and relative errors for each cycle obtained by our model and Carmeliet's are given in Table 2.

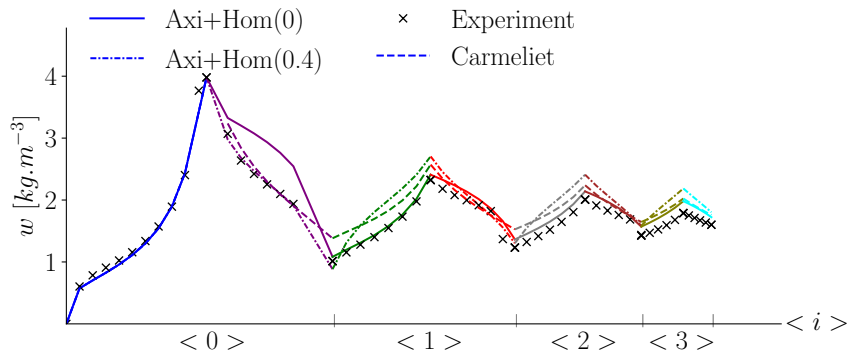

(a) Hysteresis loops with different models

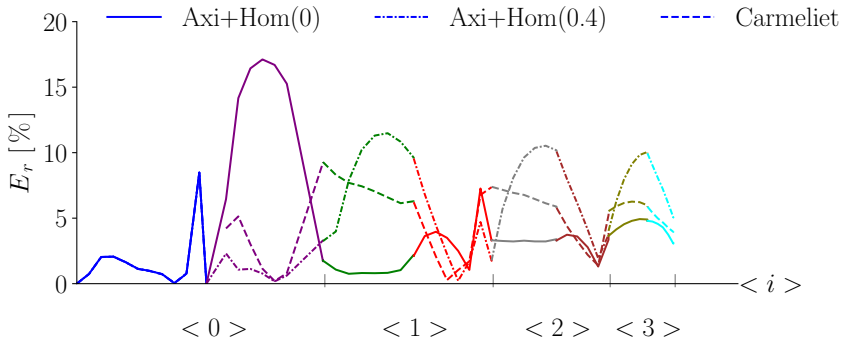

(b) Errors with experimental data

Figure 8. *Main and intermediary sorption curves of polystyrene concrete obtained experimentally and numerically (a) and their relative errors (b).*

Table 2. *Mean absolute and relative errors for the* CARMELIET *and Axisymmetric+Homotopic models compared to the experimental measures of the water content in polystyrene concrete.*

	Sorption curves	$w_{a,0}$	$w_{d,0}$	$w_{a,1}$	$w_{d,1}$	$w_{a,2}$	$w_{d,2}$	$w_{a,3}$	$w_{d,3}$
$E_g\ [\mathrm{kg.m^{-3}}]$	CARMELIET	0.37	0.72	0.87	0.59	0.74	0.45	0.63	0.50
	Axi+Hom ($s=0$)	0.37	1.50	0.16	0.45	0.36	0.33	0.47	0.43
	Axi+Hom ($s=0.4$)	0.37	0.21	1.09	0.55	0.98	0.63	0.88	0.78
$E_r\ [\%]$	CARMELIET	5.30	9.60	17.00	10.60	16	9.80	14.80	11.30
	Axi+Hom ($s=0$)	5.30	20.00	3.10	8.10	7.80	7.30	11.10	9.60
	Axi+Hom ($s=0.4$)	5.37	2.99	21.40	10.05	21.27	13.82	20.81	17.59

Table 3. *Parameters of the Van-Genuchten model to fit the experimental main sorption curves of the tested materials. The parameters of the main desorption curves were used only for Carmeliet's model.*

	main adsorption		main desorption		
	m	$\alpha/10^7$	m	$\alpha/10^7$	s
Hard Stone	0.284	1.865	0.389	4.061	0.5
Argil	0.280	0.170	0.235	0.464	0.86
Brick	0.3712	1.545	0.412	4.104	0.9
Raw earth	0.379	1.472	0.393	3.107	0.9
OSB1	0.38	2.2	0.441	4.524	0.9

3.2 Series of hysteresis predictions for different materials

To show how the model is applicable on various types of materials, further investigations were conducted on different materials, and experiments were performed to find the main and intermediary sorption curves. The Axisymmetric+Homotopic model was then used to compare the hysteresis loops obtained from the experimental results with these given by the physical model of Carmeliet. As a start, the Van-Genuchten model was used to fit the experimental main adsorption curves, where the fitted curves were used in the Axisymmetric+Homotopic model to predict hysteresis loops for each case. The types of materials and their fitted parameters related to the Van-Genuchten model are presented in Table 3. The fitted parameters relative to the experimental main desorption curves were also included as they were used in Carmeliet's model. To this end, the fitted parameter s for each material is also presented in the last column of Table 3 in order to test the efficiency of the Axisymmetric+Homotopic model.

All these materials were subjected to the same hydric dynamics conditions: the experiment started with the dried material, which underwent a wetting process until it reached 90% of external humidity, and then a drying process was applied until reaching 30% humidity level, and so on. Figure 10 presents the values that were chosen to record the loss of mass of the materials until stability was attained.

After running all the previously mentioned models, the results for the hysteresis loops are shown in Figure 9. For more details on the results, Table 4 presents the mean relative errors for the main and intermediary curves between the experimental values of water content and those obtained via the Axisymmetric+Homotopic and Carmeliet's model, and this was done for the five types of material.

As we can see from Table 4, the Axisymmetric+Homotopic model, with $s = 0$, presents an error between 20% and 35% in predicting the main desorption curve. This error was reduced drastically when calibrating the parameter s. Despite the fact that Carmeliet's model presents smaller errors (between 2% and 7.45%) in the main desorption curve, the errors produced in predicting the intermediary curves using the Axisymmetric+Homotopic model were in the same range as those produced using Carmeliet's: this was the case for OSB1 and Brick, and the error was even less in the case of Argil and hard stone. However, the errors produced with $s = 0$ varied depending on the material, ranging between 8% and 12% for Hard stone and OSB1, while spanning a range of $20 - 50\%$ in the rest of the tests.

To conclude these experiments, despite the fact that taking $s = 0$ in the Axisymmetric+Homotopic model produces results that fail to capture the main desorption curves in the first loop, the experimental tests showed that it was able to predict intermediary curves for various types of materials. However, the results, with calibrated $s \in]0, 1]$ by the main sorption curves, were in the same range as the results obtained with other models available in the literature. This proves the relevance between the prediction of hysteresis loops and the full version of Axisymmetric+Homotopic model.

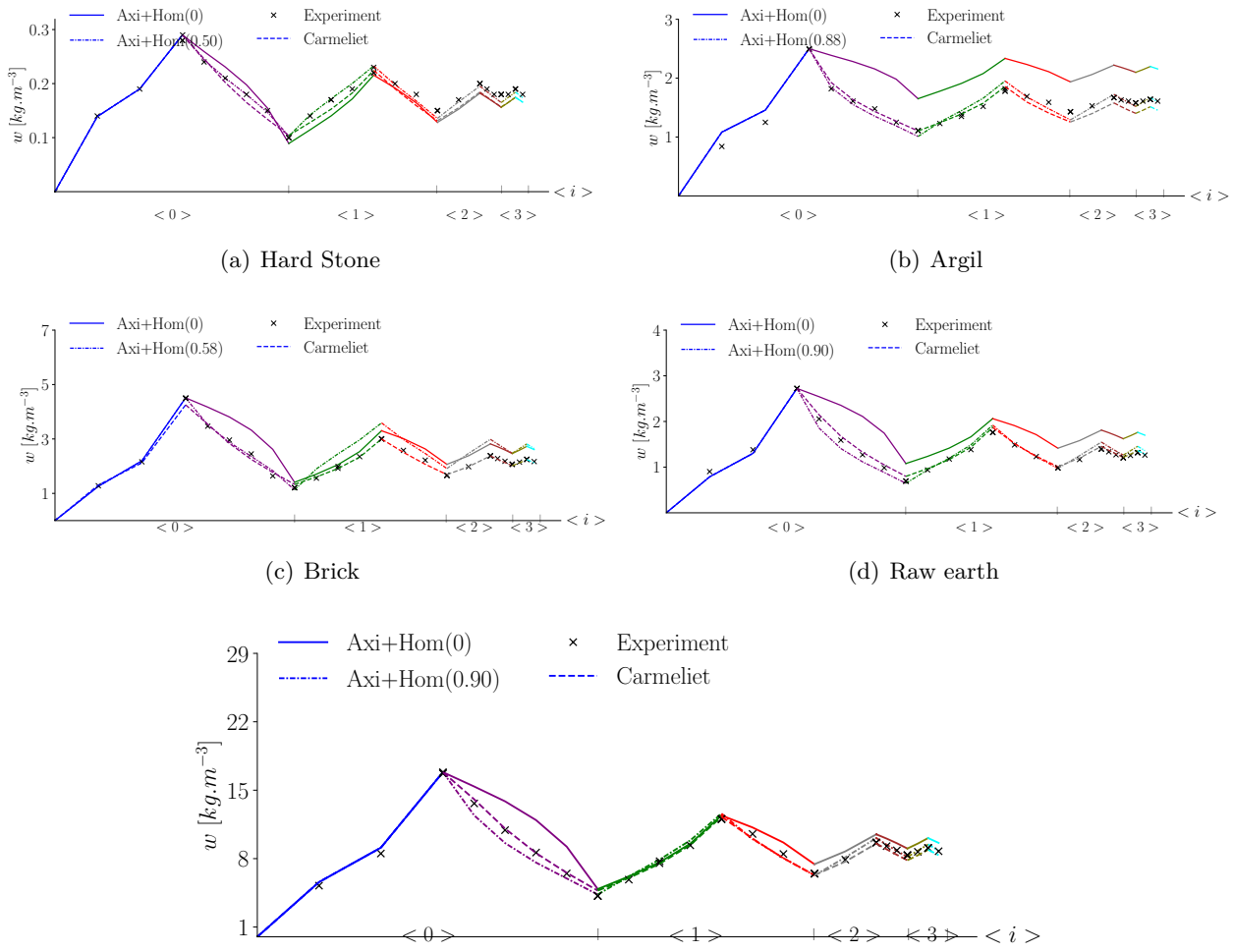

(a) Hard Stone

(b) Argil

(c) Brick

(d) Raw earth

(e) OSB

Figure 9. *Plot of the hysteresis phenomenon of the experimental main and intermediary sorption curves for different types of materials: comparison between the Axisymmetric+Homotopic and* Carmeliet.

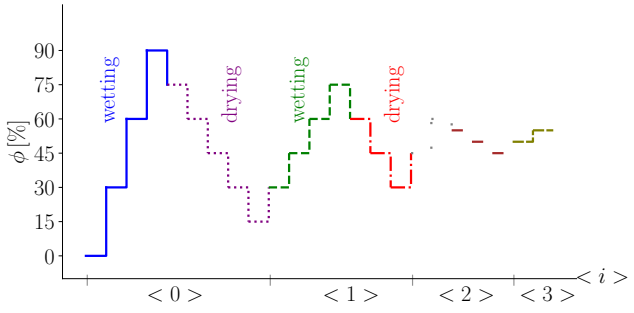

Figure 10. *Dynamics] hydric conditions used in the experiments to record water content.*

4 Modelling of mass transfer under hysteresis phenomenon

This section presents the inclusion of the hysteresis phenomenon in the modelling of mass transfer in porous materials. First, we establish the equation that governs the change in relative humidity of porous materials. Then, we present a numerical scheme that approximates this equation. We end by incorporating the effect of hysteresis into this model.

4.1 Model of heat and mass transfer

We will use the law of mass conservation in order to build the equation that governs the variation in relative humidity in porous media. Here, mass transfer occurs under isothermal conditions. The quantities w_l $\left[\mathsf{kg}\,.\,\mathsf{m}^{-3}\right]$ and w_v $\left[\mathsf{kg}\,.\,\mathsf{m}^{-3}\right]$ denote the water content in liquid and vapor phases, respectively. The equations that these functions satisfy are given as follows:

$$\frac{\partial w_l}{\partial t} \;=\; -\,\boldsymbol{\nabla}\cdot\boldsymbol{j}_l \;+\; S_l\,, \tag{26a}$$

$$\frac{\partial w_v}{\partial t} \;=\; -\,\boldsymbol{\nabla}\cdot\boldsymbol{j}_v \;+\; S_v\,, \tag{26b}$$

where $\boldsymbol{j}_l$ $\left[\mathsf{kg}\,.\,\mathsf{m}^{-2}\,.\,\mathsf{s}^{-1}\right]$ and $\boldsymbol{j}_v$ $\left[\mathsf{kg}\,.\,\mathsf{m}^{-2}\,.\,\mathsf{s}^{-1}\right]$ are the density fluxes of the liquid and vapor phases, respectively, and $\boldsymbol{\nabla}\cdot$ is the divergence operator, which is given by:

$$\boldsymbol{\nabla}\cdot := \frac{\partial}{\partial x} + \frac{\partial}{\partial y} + \frac{\partial}{\partial z}\,. \tag{27}$$

The liquid S_l $\left[\mathsf{kg}\,.\,\mathsf{m}^{-2}\,.\,\mathsf{s}^{-1}\right]$ and vapor S_v $\left[\mathsf{kg}\,.\,\mathsf{m}^{-2}\,.\,\mathsf{s}^{-1}\right]$ source terms verify $S_l \;+\; S_v \;=\; 0$, since no other source exists. Thus, by summing Eq. (26a) and Eq. (26b), one obtains:

$$\frac{\partial\left(\,w_l \;+\; w_v\,\right)}{\partial t} \;=\; -\,\boldsymbol{\nabla}\cdot\left(\,\boldsymbol{j}_l \;+\; \boldsymbol{j}_v\,\right). \tag{28}$$

The moisture content w includes both the liquid and vapor phases:

$$w \;=\; w_l \;+\; w_v\,. \tag{29}$$

The shape of the sorption curve is considered to be the same as in the Van–Genuchten model detailed in Eq. (11). Given this relation, we have:

$$\frac{\partial w}{\partial t} \;=\; \frac{\partial w}{\partial \phi}\,\frac{\partial \phi}{\partial t}\,, \tag{30}$$

Table 4. *Mean relative overall errors for the* CARMELIET *and the Axisymmetric+Homotopic models compared to the experimental measures of water content in different types of materials.*

		Sorption curves	$w_{a,0}$	$w_{d,0}$	$w_{a,1}$	$w_{d,1}$	$w_{a,2}$	$w_{d,2}$	$w_{a,3}$	$w_{d,3}$
E_r [%]	Hard stone	CARMELIET	2.74	4.60	6.81	6.87	10.06	8.96	10.72	8.16
		Axi+Hom($s=0$)	2.74	6.43	12.86	7.19	11.72	9.62	10.99	8.01
		Axi+Hom($s=0.5$)	2.74	2.02	4.02	5.18	6.24	4.23	6.25	3.11
	Argil	CARMELIET	5.57	2.71	1.74	7.78	10.34	9	10.92	9.42
		Axi+Hom($s=0$)	5.57	33.93	52.50	44.33	51.15	49.10	50.19	50.79
		Axi+Hom($s=0.86$)	5.57	6.30	10.79	8.81	7.34	6.47	4.44	6.81
	Brick	CARMELIET	2.72	5.08	7.62	5.12	6.80	4.93	4.39	5.16
		Axi+Hom($s=0$)	2.72	23.49	21.11	20.22	31.16	25.67	27.74	27.87
		Axi+Hom($s=0.9$)	2.72	9.95	6.56	6.19	7.04	7.74	6.41	8.45
	Raw earth	CARMELIET	4.37	3.68	6.60	3.93	3.68	2.49	2.86	2.85
		Axi+Hom($s=0$)	4.37	30.20	24.96	31.46	33.44	32.50	34.13	34.08
		Axi+Hom($s=0.9$)	4.37	6.69	7.76	5.49	9.21	7.70	9.03	9.34
	OSB1	CARMELIET	3.64	2.26	4.24	3.24	1.94	3.77	4.78	3.01
		Axi+Hom($s=0$)	3.64	17.51	5.53	7.63	11.77	8.52	9.52	10.79
		Axi+Hom($s=0.9$)	3.64	6.76	4.64	4.61	3.74	3.46	2.68	3.42

with

$$\frac{\partial w}{\partial \phi} = \frac{\rho_2 R T \pi}{M_2 \phi} \frac{1}{\left(1 + \left(-\alpha^{-1} \cdot h\right)^{\frac{1}{1-m}}\right)^{m+1}} \cdot \frac{\alpha^{-1} m}{m-1} \left(-\alpha^{-1} . h\right)^{\frac{m}{1-m}} . \tag{31}$$

Thus, Eq (28) becomes:

$$\frac{\partial w}{\partial t} = -\boldsymbol{\nabla} \cdot \left(\boldsymbol{j}_l + \boldsymbol{j}_v\right). \tag{32}$$

Now, the density fluxes are derived. The transfer of the liquid phase is governed by the gradient of capillary pressure, which is obtained by the application of DARCY's law. Using KELVIN's law, which links the capillary pressure to relative humidity, the liquid fluxes can be expressed by:

$$\boldsymbol{j}_l = -K_l \boldsymbol{\nabla} \phi , \tag{33}$$

where K_l $\left[\mathsf{kg} . \mathsf{m}^{-1} . \mathsf{s}^{-1}\right]$ is the liquid transfer coefficient and ∇ is the gradient operator. This depends on the moisture content w according to the following formula:

$$K_l(w) = K_0 k_r(w) , \tag{34}$$

where K_0 is the intrinsic permeability coefficient that is considered in this model, and k_r is the relative permeability taken as defined in [44]. The coefficient k_r depends on the moisture content w as given below:

$$k_r(w) = \sqrt{w}\left(1 - \left(1 - w^{1/m}\right)^m\right)^2 , \tag{35}$$

with m being the parameter of the VAN–GENUCHTEN model. Similarly, the vapor flux is given by:

$$\boldsymbol{j}_v \;=\; -K_v\,\boldsymbol{\nabla}\phi\,, \tag{36}$$

where K_v $\left[\,\mathsf{kg}\,.\,\mathsf{m}^{-1}\,.\,\mathsf{s}^{-1}\,\right]$ is the vapor transfer coefficient under a relative humidity gradient. It is determined from the measured properties of the material. In the end, the model of mass transfer can be written as:

$$\frac{\partial w}{\partial \phi}\,\frac{\partial \phi}{\partial t} \;=\; \boldsymbol{\nabla}\cdot\Big(\,(K_l \;+\; K_v)\,\boldsymbol{\nabla}\phi\,\Big)\,. \tag{37}$$

To complete the model, the Fourier boundary conditions are considered as mentioned below, where h is the convection coefficient that is determined using parametric identification, and ϕ_∞ is the relative humidity of ambient air

$$(K_l \;+\; K_v)\,\boldsymbol{\nabla}\phi = h\,(\phi \;-\; \phi_\infty)\,. \tag{38}$$

4.2 Numerical model

In order to solve numerically equation (37), the Finite Elements Method was used for space discretization, and an adaptive Euler implicit discretization for the time variable.

4.2.1 Space discretization.

Let us consider that the solution is written as a finite sum of functions φ of order 1

$$\phi\,(t\,,\,x\,) \;=\; \sum_{n\,=\,0}^{Nx}\,\phi_n(t)\;\varphi_n(x)\,, \tag{39}$$

where $\phi_n(t\,)$ is the change in the value of the solution at the node x_n on the mesh Ω_x. Here, $\phi_n(x)$ are the basic elements of the function space of the solution. The weak formulation was used to take into account the boundary conditions. The finite element solver in the FEniCS project [45] was used to implement and solve equation (37).

4.2.2 Time integration.

In numerical time integration for dynamical systems, it is very important to be careful with the integration part when it comes to stiff equations [46, 47], and especially when it comes to large time dynamics [48], as in the model of heat and mass transfer. Numerical schemes were massively developed to simulate the time evolution of the solution. Different strategies were considered: from searching for the solution in a discrete space of time, where the simplest scheme is the first order Euler explicit scheme, to finding an approximation in a continuous time space, where the solution is written as a time series expansion [49]. For the above mass transfer problem (37), an implicit scheme, with assistance of a fixed point problem [50], was developed to ensure stability for the solution with high dynamics. We will now present the semi-discrete equation we solved to get the variation in time of the solution. The solution was calculated at a discrete value of time t_j. Let us suppose that the solution $\phi\,(t_j\,) \;=\; \phi^j$ is known at time $t \;=\; t_j$, and we want to find an approximation of ϕ^{j+1} at $t \;=\; t_j \;+\; \Delta t_{j-1}$. With a progressive Taylor series expansion of order 1, the approximation will be:

$$\begin{aligned} f(\,\phi^j\,)\,\frac{\phi^{j\,+\,1} \;-\; \phi^j}{\Delta t_{j-1}} \;&=\; \nabla.\,\Big(\,(K_l \;+\; K_v)\nabla\phi^{j+1}\,\Big), \\ f(\,\phi^j\,) \;&=\; \frac{\partial w}{\partial \phi}\,(\,\phi^j\,). \end{aligned} \tag{40}$$

To find ϕ^{j+1}, we write the above equation in the form of a fixed point problem [50] as follows:

$$\phi^{j+1} = \frac{\Delta t_{j-1}}{f(\phi^j)} \nabla \left((K_l + K_v) \nabla \phi^{j+1} \right) + f(\phi^j)\, \phi^j . \tag{41}$$

Thus, the unknown ϕ^{j+1} is the solution to a nonlinear equation for which a fixed-point algorithm [50] is used to find a solution. Throughout this resolution, we will be able to compute the adaptive time step for the next iteration.

Adaptive time step To solve the non-linear equation:

$$\phi^{j+1} = F(\phi^{j+1}), \tag{42}$$

the fixed-point algorithm [50] was employed: it is based on the computation of a series of functions ϕ_k^j that converges to the exact solution of the equation. The series is defined by:

$$\phi_{k+1}^{j+1} = F(\phi_k^{j+1}). \tag{43}$$

We stop when the error between two consecutive functions verifies the following inequality:

$$|| \phi_{k+1}^{j+1} - \phi_k^{j+1} || = \varepsilon_k^j \leqslant \varepsilon , \tag{44}$$

where ε is a user-defined threshold. Once the condition is verified, $\phi(t_j + \Delta t_{j-1})$ is approximated by the obtained value ϕ_k^{j+1}. The error computed at the end of the fixed-point algorithm will be used to predict the new time step for the next time integration:

$$\Delta t_j = \Delta t_{j-1} \min\left(2, \max\left(\left(\frac{10^{-p}}{\varepsilon_k^j} \right)^{\frac{1}{p}}, 0.3 \right) \right), \tag{45}$$

where p is the desired precision to be maintained during the computation. The minimal and maximal factors used to bound the adaptive step were 0.3 and 2, respectively.

4.3 Integration of the hysteresis phenomenon

Once the direct problem (37) is established and the adsorption curve is defined based on experimental data, it can be simulated under dynamical boundary conditions. To incorporate the hysteresis effect into the model, a binary condition is set to specify if the material is undergoing an adsorption or desorption process. This condition does not affect the solver that produces the numerical solution. This binary condition is incorporated into the equation as follows:

$$w = \frac{1}{2}\left(1 + \operatorname{sign}\left(\frac{\partial \phi_\infty}{\partial t}\right)\right) \mathcal{T}_{a,s}(\phi) + \frac{1}{2}\left(1 - \operatorname{sign}\left(\frac{\partial \phi_\infty}{\partial t}\right)\right) \mathcal{T}_{d,s}(\phi). \tag{46}$$

This equation is included in the model of of Heat and Mass transfer to take into account the hysteresis phenomenon and the continuity property. Once computed, it is used to determine the water content in equation (37), and more specifically in Eqs. (11), (31) and (34).

To this end, we present the strategy in the flow chart in Figure 11 when the Axisymmetric+Homotopic model is employed. We started by fitting the experimental main adsorption and desorption data with a given model (here it is the Van-Genuchten model) to obtain its parameters (here m and α) and the parameter s related to the Axisymmetric+Homotopic model by minimizing the error with the experimental data.

These parameters were used in the Axisymmetric+Homotopic model in order to predict the intermediary sorption curves $w_{a/d,i}$ regarding the given dynamics conditions at different instants T_i. The following loop was repeated at every instant T_i: at every inversion point T_i, we defined the type of process, whether it was a wetting or drying, then we used the associated sorption curve $w_{a,i}$ or $w_{d,i}$. This curve was then incorporated into the hygrothermal model given in equation (37) and the problem was simulated between $[T_{i-1}, T_i]$ with the proposed schemes and numerical tools. We note that the Axisymmetric+Homotopic model is not limited to these schemes, others could be employed. At the end of the simulation, the values of the water content for each nodal point in the material were calculated. Then, we prepared for the next iteration by computing the coefficients s_a or s_d and applying the transformation $T_{d\,,\,s}$ or $T_{a\,,\,s}$, and so the loops carried on.

In the next section, a comparison between the numerical simulations, using this procedure, and experimental measurements will be presented to show the relevance of the proposed model to reality.

5 Mass transfer with the hysteresis phenomenon

In the following, the effect of taking into account the hysteresis phenomenon on mass transfer in porous materials is described. A comparison between numerical simulations (with and without the hysteresis phenomenon) and experimental output is also shown. Two types of materials were studied: hemp concrete and aerated lime (Tradical ® PF70), which were preconditioned at a relative humidity of 50 % until mass stabilization. Note that, for the second case, a comparison with a model from the literature was made.

5.1 First test: hemp concrete

The hemp concrete used for this test was obtained by mixing defined quantities of hemp shives, aerated lime binder (Tradical PF70) and water according to the implementing rule for hemp concrete [51]; it had an average density of about 484 $\mathsf{kg\,.\,m^{-3}}$. The porosity of the sample $\pi = 0.71$ was obtained by using the water porosity test. To produce an experimental observation of mass transfer and compare this with the numerical predictions, a cubic sample with sides of 10 cm was used. It was covered with aluminium adhesive tape on 5 of its sides to ensure a one-directional transfer (see Figure 12). Relative humidity and temperature sensors were inserted at a position 2.5 cm away from the exposed surface. The material was subjected to dynamic conditions of wetting and drying cycles over 12 days. The experimental results are presented in Figure 13.

Then, to obtain the main adsorption curve for the Axisymmetric+Homotopic model, the Van–Genuchten model (11) was used. The parameters were identified using the first strip of the experimental values. We obtain the following fitted parameters:

$$m = 0.41, \qquad \alpha = 2.10 \times 10^7, \qquad s = 0. \tag{47}$$

To find the parameter s, the second strip of the experimental data is used i.e., the wetting cycle that happens during the time interval $[72, 144]$ $[\,\mathsf{hours}\,]$. Here, we found that $s = 0$ is the optimum parameter that fits the the homotopic function in order to be close to the experimental data. The second cycle in the experimental outputs was then reproduced numerically. This experiment enabled us to highlight the effect of the hysteresis phenomenon in the hydric behaviour of the material.

In order to better show the effect of this phenomenon, the numerical output of both simulations (with and without hysteresis) and the experimental output are shown in Figure 14. In this Figure, it is clear that neglecting the hysteresis phenomenon leads to a difference between the numerical simulation and the experimental results with a maximum relative error of about 5 %. However, the inclusion of this phenomenon in the model, using the Axisymmetric+Homotopic model, improved the quality of the prediction and, consequently, reduced the discrepancies between the numerical and the experimental results to about 1 %. These results show, on one hand, the relevance of the proposed hysteresis model to reality, and on the other, the importance of taking into account this phenomenon in the mass transfer model to improve its prediction quality.

Table 5. *Local errors between numerical and experimental outputs: Effect of the hysteresis phenomenon.*

$\epsilon\,(t_r)$ [%] $\diagdown$ t_r [hours]	72	105	144	180	252	288
Without hysteresis	0.23	−4.78	−3.58	−2.27	−5.17	−3.98
With hysteresis	0.23	−0.81	−0.9	−0.35	−1.94	−1.63

Table 6. *Overall error between numerical and experimental outputs: Effect of the hysteresis phenomenon.*

$\epsilon_{[\,a\,,\,b]}$ [%] $\diagdown$ $[a, b]$ [hours]	$[0, 72]$	$[72, 144]$	$[144, 216]$	$[216, 288]$
Without hysteresis	0.71	3.37	2.09	3.73
With hysteresis	0.71	0.73	0.38	1.1

To analyze these results, the local (ϵ) and overall ($\epsilon_{[\,a\,,\,b]}$) errors between the experimental and numerical outcomes (with and without hysteresis) are presented in Tables 5 and 6, respectively. Note that the integral operation in the overall error is approximated by the trapezoid method since the experimental values $\hat{\phi}^{\,r} = \hat{\phi}\,(\,t_r\,)$ are discontinuous. Hereafter, the local and mean $L^2\,(\,[\,a\,,\,b\,]\,)$ errors are given by the following formulas:

$$\epsilon\,(t_r) = \phi(t_r) - \phi^{r}\,(t_r), \tag{48}$$

$$\epsilon_{[\,a\,,\,b]} = \frac{1}{b-a}\sqrt{\int_a^b \left(\phi\,(t) - \hat{\phi}\,(t)\right)^2 dt}\,. \tag{49}$$

Based on these results, it is clear that taking into account the hysteresis phenomenon reduces significantly the discrepancies between the experimental and numerical results. For example, an overestimation, of about 4.78 % at $t = 105h$, of the relative humidity was recorded when the hysteresis phenomenon was omitted. This overestimation was reduced to 0.81 % by integrating this phenomenon in the model. Moreover, in the second cycle (at time $t = 252$ h), the overestimation of the relative humidity profiles seems greater compared to the first cycle: an error of 5.17 % was recorded when the hysteresis phenomenon was neglected. This error was reduced to 1.9 % by including the intermediary loops between the adsorption and desorption phases.

5.2 Second test: aerated lime (Tradical ® PF70)

In this section, the numerical and experimental results for Tradical® PF70 are presented. This material has a density of 1172 $\mathsf{kg\,.\,m^{-3}}$ and a porosity of about 50 %. The experiment was carried out on a cubic sample of dimensions $15 \times 15 \times 5$ cm^3, where 5 of its sides were isolated. The material was subjected to drying cycles at 33 % and wetting at 75 %. A relative humidity sensor was placed at a depth of 2.5 *cm* in order to record the experimental data, which were then used to test the efficiency of the model. The test was conducted at a temperature of $23°C$. This experiment was performed to show that the proposed model could be applied to other types of materials.

In addition to a comparison with the experimental data, Carmeliet's model [33] was programmed and applied in our machine, and its output data was used to compare the performance of our model to that of models in the literature. Equation (11) was used to model the main adsorption curve for the Axisymmetric+Homotopic model and Carmeliet's.

5.2.1 Parameters of the model in equation (37).

To start the simulation, we used the model in equation (11) to fit the main adsorption curve to run both hysteresis models. The parameters were fitted with the main experimental adsorption curve of the material using a least square method. The results are presented in the second row of Table 7. The experimental main desorption curve was fitted, on one hand, with equation (11) to get the parameters of the main desorption

curve for CARMELIET's model (see third row of Table 7), and on the other hand, to fit the parameter s for the Axisymmetric+Homotopic model. We found out that $s = 0$. Thus, equation (37) was simulated

Table 7. *Parameters used to fit the VAN-GENUCHTEN model with the experimental main adsorption and desorption curves of the Tradical® PF70 .*

	m	α
main adsorption	0.45	1.3×10^7
main desorption	0.3	2.1×10^7

using the above parameters for CARMELIET's model and the main adsorption curves with $s = 0$ for the Axisymmetric+Homotopic one.

To fulfill the elements of equation (37), the intrinsic permeability coefficient K_0 and the convective coefficient h were identified on a strip of experimental results. Their values are given as follows:

$$K_0 \;=\; 5.1 \times 10^{-18} \big[\,\mathsf{m.s}^{-2}\,\big], \qquad\qquad h \;=\; 8 \times 10^{-5} \big[\,\mathsf{m.s}^{-1}\,\big]. \tag{50}$$

5.2.2 Dynamic conditions.

The simulation time was about 12 days, during which the sample was exposed to 9 cycles of drying at 33% relative humidity and wetting at 75%. After 32 hours of stabilization, the first 5 cycles were completed: they consisted of 8 hours of drying followed by 4 hours of wetting. The last 4 drying and wetting cycles had the same time lapse, which was 24 hours. The results are presented in Figure 15.

5.2.3 Results and discussions.

Based on these experiments, it has been shown that failing to take into consideration the hysteresis phenomenon produces results that diverge from the experimental ones. However, when this phenomenon is taken into account, the numerical results agree perfectly with those of the experiment, where the maximum deviation was reduced from 8 %, when only the main adsorption curve was considered in the model, to 2 % when hysteresis was taken into account using the Axisymmetric+Homotopic model (Figure 16).

To show some details of the error with each model, some points in Figure 15 were picked out, and their relative local error compared with the experimental results computed and presented in Table 8. The errors of the Axisymmetric+Homotopic (Axi+Hom) and the CARMELIET model were consistent.

Table 8. *Local error between experimental and simulation results using different models.*

ϵ [%] $\diagdown$ t_r [hours]	32	44	56	68	80	104	128	152	176	200	248
W/O hyst ($w_{a,0}$)	-2.00	-1.91	-2.00	-2.27	-2.56	-7.08	2.90	-5.61	2.69	-5.93	-6.18
W/O hyst ($w_{d,0}$)	-1.80	-1.51	-1.33	-1.27	-1.23	-3.55	2.36	-2.36	2.80	-2.50	-2.84
W/ hyst (CARMELIET)	0.22	0.53	0.71	0.75	0.77	0.78	0.47	0.11	-0.09	-0.71	-1.00
W/ hyst (Axi+Hom(0))	-0.73	-0.38	-0.21	-0.19	-0.37	-0.84	-0.01	-0.41	0.68	0.14	0.62

Moreover, Table 9 shows that the mean L^2 deviation errors over different intervals, obtained with our model or with CARMELIET's model, compared to the experimental results, do not exceed 0.24 and 0.23 (24% and 23%), respectively. Therefore, the mean L^2 deviations across all the simulation times were about 0.06 (6%) for the Axisymmetric+Homotopic model and 0.05 (5%) for CARMELIET's, which means that our model produced numerical simulations close to a reference model, and confirmed the hypothesis that taking into account the hysteresis phenomenon reduces the errors.

In order to better show the relevance of the results, the continuous errors of all these simulations (with and without hysteresis) have been added in Figure 16. In conclusion, the hysteresis model refined the

error between the numerical and experimental results, and improved the quality of prediction of the hydric behaviour of porous materials.

Table 9. *Mean $L^2([a,b])$ error between experiment and simulation results using different models.*

$\epsilon_{[a,b]}$ ╲ time [hours]	[28,63[	[63,88[	[88,136[	[136,184[	[184,232[	[232,280[	[28,280[
W/O hyst ($w_{a,0}$)	0.25	0.38	0.68	0.55	0.57	0.66	0.23
W/O hyst ($w_{d,0}$)	0.18	0.17	0.37	0.33	0.31	0.32	0.13
W/ hyst (Carmeliet)	0.15	0.23	0.1	0.07	0.09	0.11	0.05
W/ hyst (Axi+Hom(0))	0.08	0.08	0.08	0.1	0.16	0.24	0.06

6 Conclusion

In this work, a new mathematical model of the hysteresis phenomenon was developed and validated. It is based on the assumption that the adsorption and desorption curves are axisymmetric. This approach makes the modelling part easier as it only requires one of the main sorption curves. When both main sorption curves were available, the model was updated by integrating a homotopic function that could deform the axisymmetric function and bring the prediction of the main desorption curve closer to the experimental value by adjusting a parameter s. The Axisymmetric+Homotopic model was implemented in numerical simulation tools in a non-intrusive way, and it ensured a better quality of prediction relative to the experimental results.

Taking into consideration the axisymmetric hypothesis between both sorption curves allowed us to reduce the experimental data needed in the simulation phase. Indeed, the model needs only one main sorption curve, which can be determined from the experimental values, or by inverse problem techniques using a strip of experimental data. The second main curve was identified by a mathematical transformation of the first. This transformation was defined and generalized to ensure a continuity property in dynamic boundary conditions, and this continuity reflected the hydric history of the material. The applicability of the Axisymmetric+Homotopic ($s = 0$) model was tested on the production of main and the intermediary sorption curves for various types of materials, and the results show that the model could predict hysteresis phenomenon for some classes. The model has an additional property that can be used for a wide range of materials by incorporating the homotopy function. A comparison with sorption curves produced in experiments showed that the Axisymmetric+Homotopic model contributes by predicting hysteresis loops for all the tested materials, and the results were in the same range as the reference model.

Moreover, the model was also compared with one from the literature, namely, Carmeliet's model. Our model was able to reproduce accurately the experimental data with relatively negligible deviations compared to Carmeliet's.

The Axisymmetric+Homotopic model is well designed for predicting hysteresis loops. Although when $s = 0$, the proposed model produces results that may capture approximately the main desorption curve for some types of materials, the full version of the Axisymmetric+Homotopic model provides better prediction results due to the homotopic parameter. Experimental tests showed that it could predict intermediary sorption curves with errors that are in the same range as those produced by other models in the literature. Finally, this work constitutes an important step towards taking into account the hysteresis phenomenon in the modelling of the hygrothermal behaviour of building materials.

Acknowledgments

The Region and the European Union supported the < CPER-FEDER Bâtiment durable Axis 2 MADUR Project: High-performance building materials with low environmental impact, sustainable and resilient > within the framework of the ≪ Operational FEDER/FSE 2015-2020≫ and Energy saving certificate program of the Ministry of Ecological and Solidarity Transition "SmartReno support " 2019-2021.

References

[1] Rafik Belarbi, Menghao Qin, Abdelkarim Aït Mokhtar, and Lars Olof Nilsson. Experimental and theoretical investigation of non-isothermal transfer in hygroscopic building materials. *Building and Environment*, 43(12):2154 – 2162, 2008. 1

[2] Menghao Qin, Rafik Belarbi, Adbdelkarim Aït Mokhtar, and Francis Allard. Simulation of coupled heat and moisture transfer in air-conditioned buildings. *Automation in Construction*, pages 624–631, 08 2009. 1

[3] Véronique Baroghel-Bouny. Water vapour sorption experiments on hardened cementitious materials. part ii: Essential tool for assessment of transport properties and for durability prediction. *Cement and Concrete Research*, 37(3):438 – 454, 2007. Cementitious Materials as model porous media: Nanostructure and Transport processes. 1

[4] Menghao Qin, George Walton, Rafik Belarbi, and Francis Allard. Simulation of whole building coupled hygrothermal-airflow transfer in different climates. *Energy Conversion and Management*, 52(2):1470 – 1478, 2011. 1

[5] Jerzy Kwiatkowski, Monika Woloszyn, and Jean Jacques Roux. Modelling of hysteresis influence on mass transfer in building materials. *Building and Environment*, 44(3):633 – 642, 2009. 1, 2

[6] Hannelore Derluyn, Dominique Derome, Jan Carmeliet, Eric Stora, and Rémi Barbarulo. Hysteretic moisture behavior of concrete: Modeling and analysis. *Cement and Concrete Research*, 42(10):1379 – 1388, 2012. 2

[7] Xiaobo Zhang, Wolfgang Zillig, Hartwig M. Künzel, Christoph Mitterer, and Xu Zhang. Combined effects of sorption hysteresis and its temperature dependency on wood materials and building enclosures-part i: Measurements for model validation. *Building and Environment*, 106:143–154, 2016.

[8] Georges Costantine, Chadi Maalouf, Tala Moussa, Elias Kinab kinab, and Guillaume Polidori. Hygrothermal evaluation of hemp concrete at wall and room scales: Impact of hysteresis and temperature dependency of sorption curves. *Journal of Building Physics*, 44(3):183–224, 2020. 1, 2

[9] Abdelakrim Trabelsi, Rafik Belarbi, Philippe Turcry, and Abdelakrim A¨ Mokhtar. Water vapour desorption variability of in situ concrete and effects on drying simulations. *Magazine of Concrete Research*, 63(5):333–342, 2011. 1

[10] Abdelkrim Trabelsi, Ameur Hamami, Rafik Belarbi, Philippe Turcry, and Abdelkarim A¨-Mokhtar. Assessment of the variability of moisture transfer properties of high performance concrete from a multi-stage drying experiment. *European Journal of Environmental and Civil Engineering*, 16(3-4):352–361, 2012. 1

[11] Jose Antonio de Almeida Neto. *Transport d'humidité en matériau poreux en présence d'un gradient de température : caractérisation expérimentale d'un béton cellulaire*. PhD thesis, Université Joseph Fourier (Grenoble), 1992. 1

[12] Zhidong Zhang, Mickael Thiéry, and Véronique Baroghel-Bouny. A review and statistical study of existing hysteresis models for cementitious materials. *Cement and Concrete Research*, 57:44 – 60, 2014. 2, 3

[13] Romain Rémond, Giana Almeida, and Patrick Perré. The gripped-box model: A simple and robust formulation of sorption hysteresis for lignocellulosic materials. *Construction and Building Materials*, 170:716 – 724, 2018. 1, 2

[14] Yacine Aït Oumeziane, Marjorie Bart, Sophie Moisette, and Christophe Lanos. Hysteretic behaviour and moisture buffering of hemp concrete. *Transport in Porous Media*, 103:515–533, 2014. 2

[15] Yechezkel Mualem. A conceptual model of hysteresis. *Water Resources Research*, 10:514–520, 1974. 2

[16] Yechezkel Mualem and Arcady Beriozkin. General scaling rules of the hysteretic water retention function based on mualem's domain theory. *European Journal of Soil Science*, 60:652–661, 2009.

[17] Han-Chen Huang, Yih-Chi Tan, Chen-Wuing Liu, and Chu-Hui Chen. A novel hysteresis model in unsaturated soil. *Hydrological Process*, 19:1653–1665, 2005. 2

[18] Bjorn Johanneson and Marten Janz. Two-phase moisture transport model accounting for sorption hysteresis in layered porous building constructions. *Building and Environment*, 44:1285–1294, 2009. 2

[19] Zhidong Zhang, Mickael Thiery, and Veronique Baroghel-Bouny. Numerical modelling of moisture transfers with hysteresis in cementitious materials: Verification and investigation of the effects of repeated wetting–drying boundary conditions. *Cement and Concrete Research*, 68:10 – 23, Feb 2015. 2

[20] D. Lelièvre, T. Colinart, and P. Glouannec. Hygrothermal behavior of bio-based building materials including hysteresis effects: Experimental and numerical analyses. *Energy and Buildings*, 84:617 – 627, 2014. 2

[21] R.D. Braddock, J.Y. Parlange, and H. Lee. Application of a soil water hysteresis model to simple water retention curves. *Transport in Porous Media*, 44:407–420, 2001. 2

[22] Adrian D. Werner and David A. Lockington. Artificial pumping errors in the kool-parker scaling model of soil moisture hysteresis. *Journal of Hydrology*, 325(1):118 – 133, 2006. 2

[23] Henrik Lund Frandsen, Staffan Svensson, and Lars Damkilde. A hysteresis model suitable for numerical simulation of moisture content in wood. *Holzforschung*, 61:175–181, 2007. 2

[24] B. Johannesson and U. Nyman. A numerical approach for non-linear moisture flow in porous materials with account to sorption hysteresis. *Transport in Porous Media*, 84:735–754, 2010. 2

[25] Jerzy Kwiatkowski, Woloszyn Monika, and Roux Jean Jacques. Influence of sorption isotherm hysteresis effect on indoor climate and energy demand for heating. *Applied Thermal Engineering*, 31(6):1050 – 1057, 2011.

[26] Alessandra Patera, Hannelore Derluyn, Dominique Derome, and Jan Carmeliet. Influence of sorption hysteresis on moisture transport in wood. *Wood Science and Technology*, 50:259–283, 2016.

[27] Jingbo Shi and Stavros Avramidis. Water sorption hysteresis in wood: I review and experimental patterns' geometric characteristics of scanning curves. *Holzforschung*, 71:307–316, 2017.

[28] Thomas Busser, Julien Berger, Amandine Piot, Mickael Pailha, and Monika Woloszyn. Comparative study of three models for moisture transfer in hygroscopic materials. *Transport in Porous Media*, 126:379–410, 2018.

[29] Julien Berger, Thomas Busser, Thibaut Colinart, and Denys Dutykh. Critical assessment of a new mathematical model for hysteresis effects on heat and mass transfer in porous building material. *International Journal of Thermal Sciences*, 151, 2020. 2

[30] Jesper Arfvidsson. Moisture penetration depth for periodically varying relative humidity at the boundary. *J. CIB REPORT*, 42:75–80, 2000. 2

[31] Yacine Ait Oumeziane. *Evaluation of the hygrothermal performance of a wall by numerical simulation : application to hemp concrete walls*. PhD thesis, INSA de Rennes, March 2013. 2

[32] Peter Lehmann, Fritz Stauffer, Christoph Hinz, Olivier Dury, and Hannes Fluhler. Effect of hysteresis on water flow in a sand column with a fluctuating capillary fringe. *Journal of Contaminant Hydrology*, 33(1):81 – 100, 1998. 2

[33] Dominique Derome, Hannelore Derluyn, Wolfgang Adam Zillig, and Jan Carmeliet. Model for hysteretic moisture behaviour of wood. In Carsten Rode, editor, *Proceedings of the 8th Symposium on Building Physics in the Nordic Countries*, pages 959–965, June 16-18 2008. 2, 11, 21

[34] J B Kool and J C Parker. Development and evaluation of closed-form expressions for hysteretic soil hydraulic properties. *Water Resources Research*, 23(1):105–114, 1987. 2

[35] P Scott, G Farquhar, and N Kouwen. Hysteretic effects on net infiltration. *Materials Science*, 1983. 2

[36] Pedersen Carsten Rode. Transient calculation on moisture migration using a simplified description of hysteresis in sorption isotherms. In *Proceedings of 2nd Nordic Symposium on Building Physics in the Nordic Countries*. Trondheim, Norway, 1990. 2

[37] Dylan Lelièvre. *Numerical simulation of heat and moisture transfers in a building multi-layer wall made of bio-based materials*. Theses, Université de Bretagne Sud, Jan 2015. 2

[38] A Poulovassilis. Hysteresis of pore water, an application of the concept of independent domains. *Soil Science*, 93(6):405–412, June 1962. 2

[39] Jan Carmeliet, Martin de Wit, and Hans Janssen. Hysteresis and moisture buffering of wood. In *Proceedings of the 7th Symposium on Building Physics in the Nordic Countries : Reykjavik*, pages 55–62, 2005. 3

[40] Kenneth S. W. Sing, Douglas H. Everett, R. A. W Haul, Robert A. Moscou, L.and Pierotti, Jean Rouquerol, and Teresea Siemieniewska. Reporting physisorption data for gas/solid systems. *Pure and Applied Chemistry*, 57:603–619, 1985, IUPAC. 3

[41] Douglas C. Montgomery, Elizabeth A. Peck, and Vining G. Geoffrey. *Introduction to Linear Regression Analysis*. Wiley Series in Probability and Statistics. Wiley, 5 edition, April 2012. 6

[42] Maroua Maaroufi, Fares Bennai, Rafik Belarbi, and Kamilia Abahri. Experimental and numerical highlighting of water vapor sorption hysteresis in the coupled heat and moisture transfers. *Journal of Building Engineering*, 40, August 2021. 11

[43] Maroua Maaroufi, Akli Younsi, Rafik Belarbi, and Armelle Nouviaire. Influence of recycled polystyrene beads on cement paste properties. *MATEC Web of Conferences*, 149:10–32, 2018. 12

[44] M. Th. Van Genuchten. A closed-form equation for predicting the hydraulic conductivity of unsaturated soils. *Soil Science Society of America Journal*, 44(5):892–898, 1980. 17

[45] Anders Logg, Kent-Andre Mardal, Garth N. Wells, et al. *Automated Solution of Differential Equations by the Finite Element Method*. Springer, 2012. 18

[46] Gerhard Wanner (auth.) Ernst Hairer. *Solving Ordinary Differential Equations II: Stiff and Differential-Algebraic Problems*. Springer Series in Computational Mathematics 14. Springer-Verlag Berlin Heidelberg, 2 edition, 1996. 18

[47] Ahmad Deeb, Aziz Hamdouni, and Dina Razafindralandy. Performance of borel–padé–laplace integrator for the solution of stiff and non-stiff problems. *Applied Mathematics and Computation*, 426:127118, 2022. 18

[48] Dina Razafindralandy, Vladimir Salnikov, Aziz Hamdouni, and Ahmad Deeb. Some robust integrators for large time dynamics. *Advanced Modeling and Simulation in Engineering Sciences*, 6(1):5, Mar 2019. 18

[49] Dina Razafindralandy, Aziz Hamdouni, and Ahmad Deeb. Considering factorial series as time integration method. American Institute of Physics, July 2016. 18

[50] De Joe D. Hoffman. *Numerical Methods for Engineers and Scientists*, chapter Fixed-point iterations, pages 141–145. CRC Press, New york, second edition edition, 2001. 18, 19

[51] Ferhat Benmahiddine, Fares Bennai, Rachid Cherif, Rafik Belarbi, Abdelkader Tahakourt, and Kamilia Abahri. Experimental investigation on the influence of immersion-drying cycles on the hygrothermal and mechanical properties of hemp concrete. *Journal of Building Engineering*, 32, 2020. 20

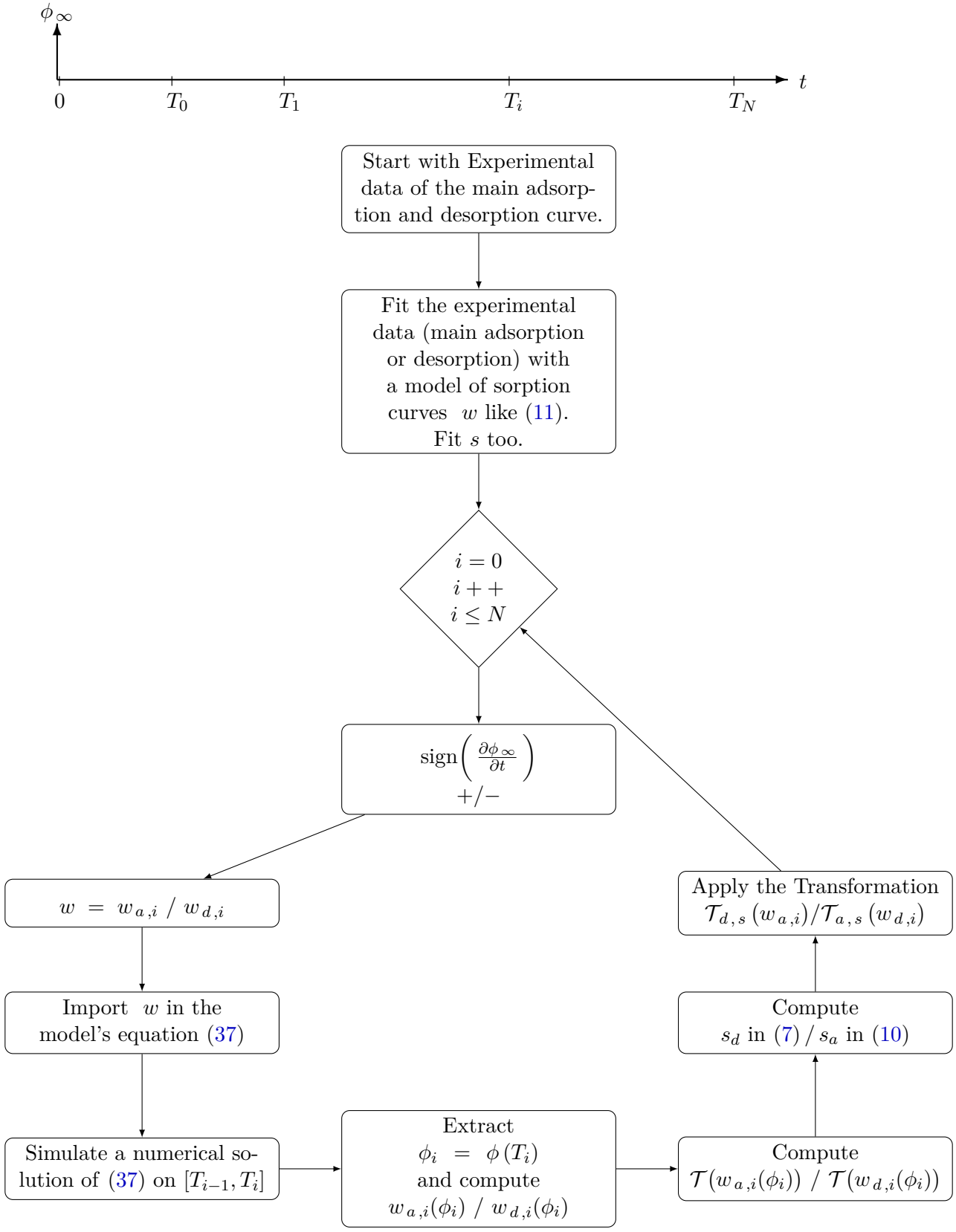

Figure 11. *Flowchart of the process used for the Axisymmetric+Homotopic model and incorporate the effect of hysteresis in the model of the variation in moisture content.*

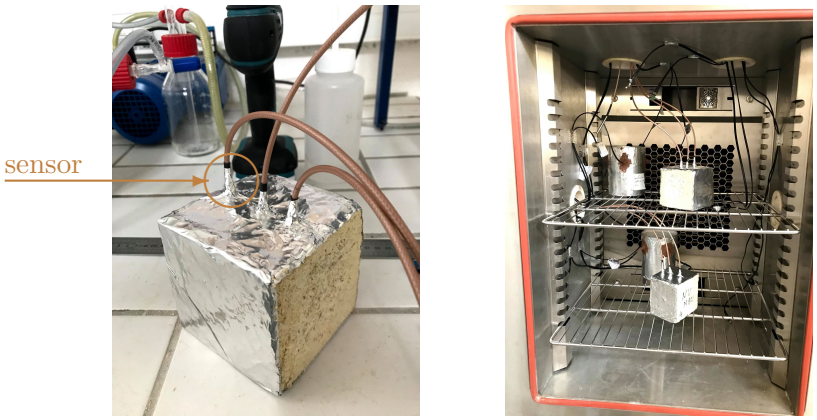

Figure 12. *Experiment used to validate the mathematical model of hysteresis: Preparing the sample* (left) *and conditioning* (right).

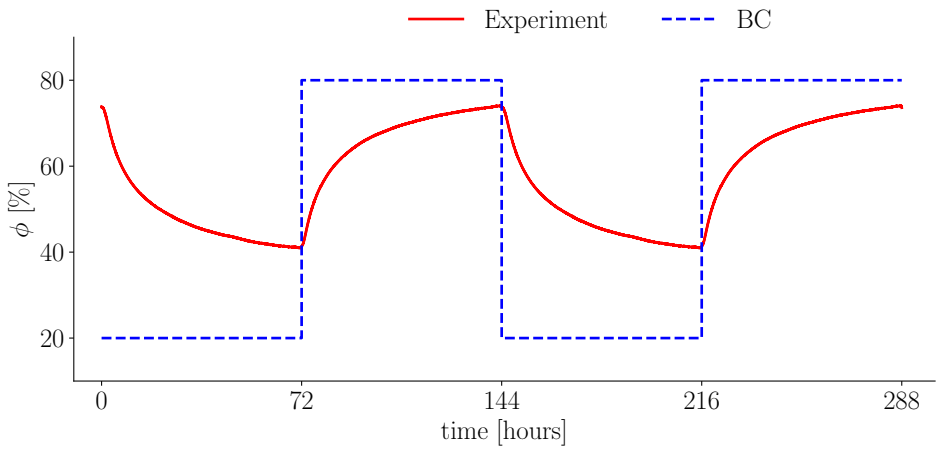

Figure 13. *Dynamic conditions of wetting and drying (dashed blue line) and experimental outputs (red line) of the relative humidity recorded on hemp concrete at position* 2.5 [cm].

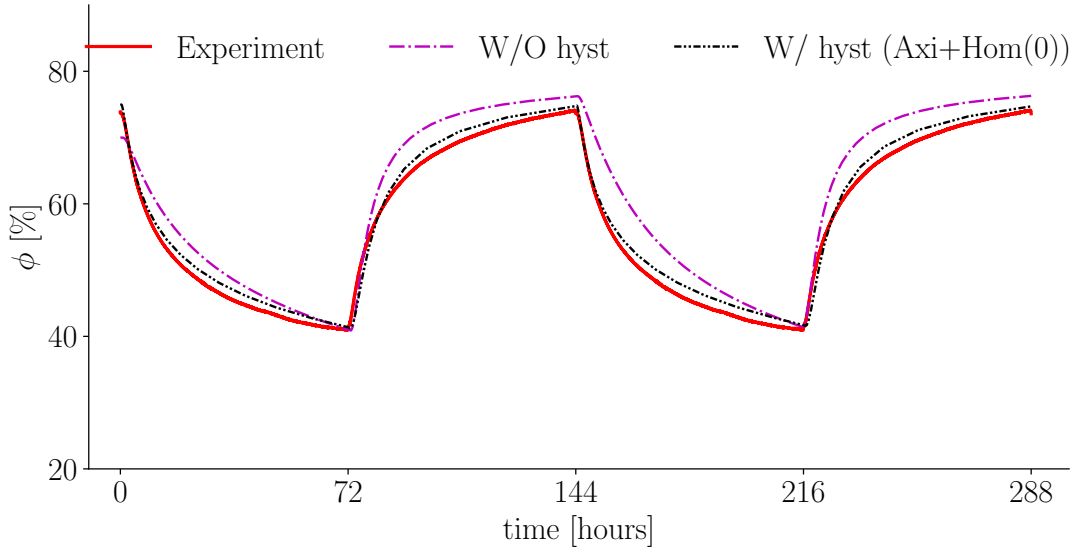

Figure 14. *Plot of Relative Humidity in the sample for two cycles of drying and and wetting.*

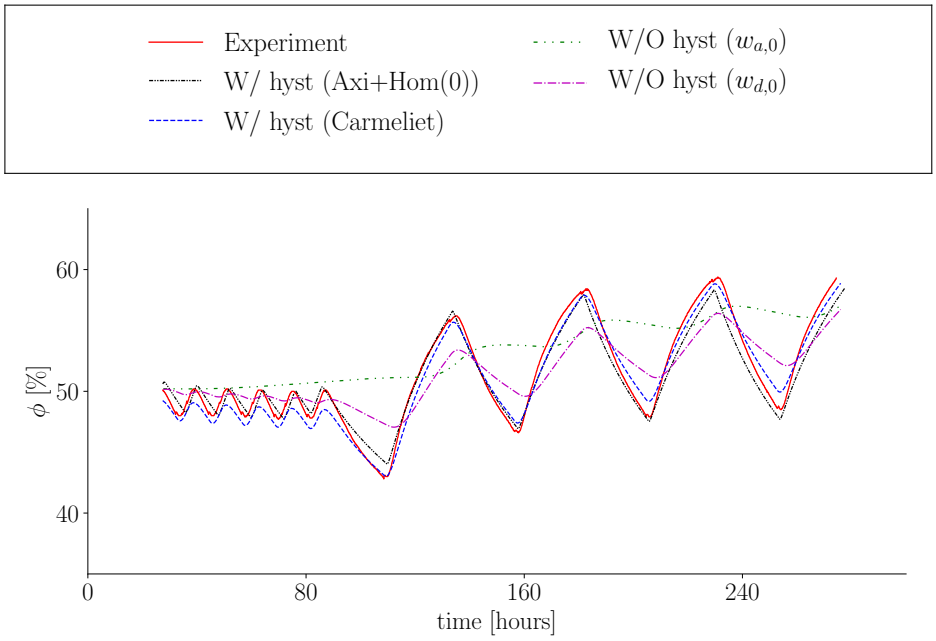

Figure 15. *Plot of the variation in relative humidity: Comparison between Experimental and numerical results with different trials.*

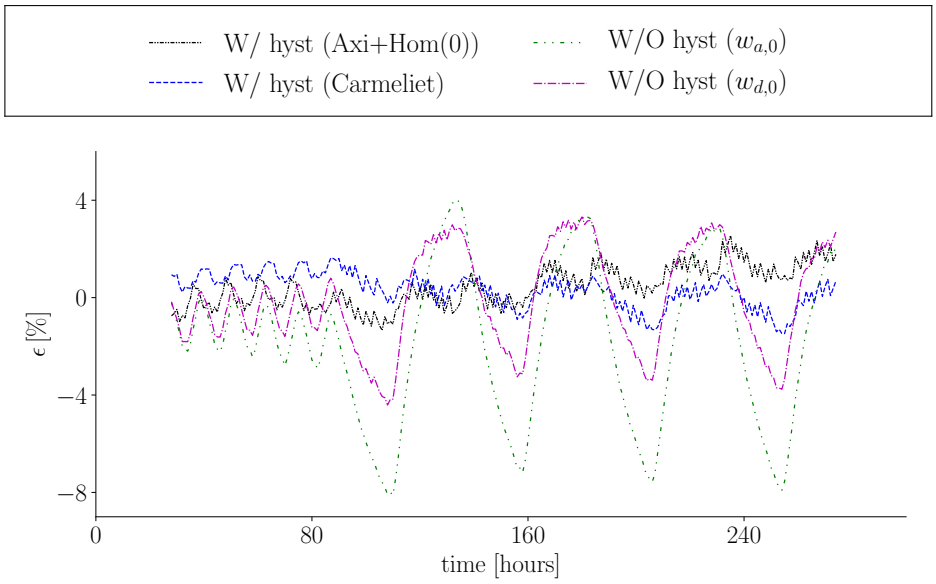

Figure 16. *Relative error between experimental and numerical values of relative humidity.*